Growth of Calcium Carbonate in the Presence of Cr(VI)

Nuria Sánchez-Pastor,*[†,‡] Alexander M. Gigler,[†,§] Juncal A. Cruz,[‡] So-Hyun Park,[†] Guntram Jordan,[†] and Lurdes Fernández-Díaz[‡,‖]

[†]Department für Geo- und Umweltwissenschaften, Ludwig-Maximilians-Universität, Theresienstrasse 41, 80333 Munich, Germany

[‡]Departamento de Cristalografía y Mineralogía, Universidad Complutense de Madrid, C/ José Antonio Nováis 2, 28040 Madrid, Spain

[§]Center for NanoScience (CeNS), Ludwig-Maximilians-Universität, Schellingstrasse 4, 80333 Munich, Germany

[‖]Instituto de Geociencias (UCM-CSIC), C/ José Antonio Nováis 2, 28040 Madrid, Spain

ABSTRACT: The extended use of hexavalent chromium Cr(VI) compounds in industrial processes caused a significant increase of the concentration of this highly toxic heavy metal in natural environments. In order to investigate the influence of Cr(VI) in the formation of $CaCO_3$, crystallization experiments were carried out in a double diffusion system, using silica hydrogel with different Cr(VI) contents as the growth medium. Crystalline products were examined by scanning electron microscopy, Raman spectroscopy, electron microprobe analysis, and single crystal X-ray diffraction. Increasing Cr(VI) concentration caused inhibition of the nucleation and growth of calcite and promoted the formation of the metastable polymorphs aragonite and vaterite. This effect correlated with a decrease of crystal size. Furthermore, the habit of calcite crystals changed with increasing Cr(VI) concentrations from {104} to forms increasingly elongated parallel to the c-axis. Raman spectroscopy, single crystal X-ray diffraction (XRD), and electron microprobe analysis (EMPA) gave strong indications of an isomorphic anion substitution of trigonal planar carbonate by the tetrahedral chromate within the calcite lattice. The apparent partitioning coefficients of Cr(VI) into calcite determined in this work suggest that the fate of this pollutant in natural environments can be significantly influenced by $CaCO_3$ precipitation processes.
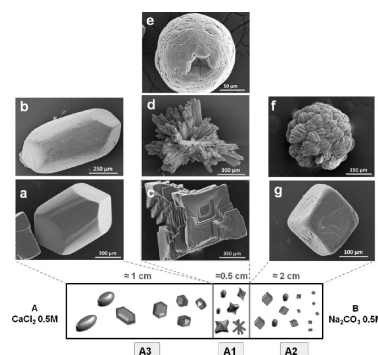
■ INTRODUCTION

Hexavalent chromium is among the most harmful heavy metals due to its mutagenic and carcinogenic properties. The extended use of Cr(VI) compounds in many industrial processes during the last century has led to a significant increase of Cr-concentration in natural environments, where it locally even exceeds safety limits.[1] Cr(VI) interacts with its chemical environment. It has been demonstrated that harmful metals can incorporate into the structure of sparingly soluble salts during growth.[2−7] Such an incorporation might also have a significant positive influence on the mobility of Cr(VI) and may contribute to the long-term reduction of its bioavailability.
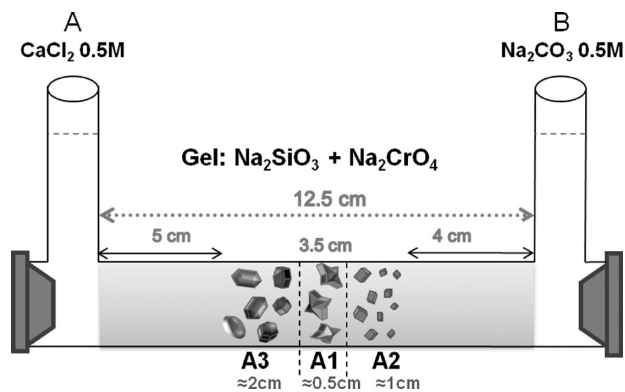
Several research groups have studied the crystallization of $CaCO_3$ in the presence of chromate. Hua et al.[8] observed that $CaCO_3$ which precipitated from chromate-bearing aqueous solution consists of a higher proportion of metastable polymorphs than $CaCO_3$ formed in a pure system without chromium. On the basis of X-ray absorp-tion near edge structure (XANES) and extended X-ray absorption fine structure (EXAFS), Tang et al.[9] concluded that chromate can substitute for carbonate within the calcite structure. In this work, we explore the role of chromate in the crystal-lization of $CaCO_3$ using the double diffusion variant of the silica hydrogel method.[10] This method is suitable for reproducing crystallization conditions similar to natural environments such as sediments and soils[11] where crystals form from confined aqueous solutions under limited mass transfer conditions.[12−14]

The goals of this research are (i) to unravel the effect of chromate anions on the polymorph selectivity of $CaCO_3$, (ii) to evaluate the ability of the $CaCO_3$ polymorph calcite, which is stable under normal Earth surface conditions, to incorporate chromate into its structure, and (iii) to understand the changes in the crystal properties of calcite induced by Cr(VI) incorporation.

■ EXPERIMENTAL METHODS

Gel Experiments. The crystallization experiments were performed in a double diffusion system. The experimental setup is shown in Figure 1. It consists of two vertical branches separated by a column of silica hydrogel. The vertical branches were filled with 0.5 M $CaCl_2$ (branch A) and 0.5 M Na_2CO_3 solutions (branch B). The silica hydrogel column was 125 mm long and 9 mm in diameter. The gel was prepared by adding 1 N HCl to a sodium silicate solution (Na_2SiO_3) (Merck KGaA, sp. gr.: 1.509 g/cm^3; pH = 11.2) until pH = 5.5 was reached. Different amounts of a Na_2CrO_4 solution were added to the mixture during the preparation of the gel. Thereby, the initial distribution of chromate within the gel column was homogeneous. Table 1 summarizes the composition of reagent solutions and the concentration of chromate in the hydrogel. Upon starting the experiments, the reactants are brought together by diffusion through the gel, and subsequently nucleation and crystal growth occur by chemical reaction within the gel column. Crystal growth was monitored by optical microscopy. Two months after

A
CaCl₂ 0.5M

B
Na₂CO₃ 0.5M

Gel: Na₂SiO₃ + Na₂CrO₄

12.5 cm

5 cm   3.5 cm   4 cm

A3   A1   A2
≈2cm ≈0.5cm ≈1cm

Figure 1. Experimental setup used for crystal growth. The sketch illustrates the different areas in which the crystallization region is divided considering the distribution of calcite crystal habits when chromate-bearing gel was used. The crystallization starts in area 1. Subsequently, crystals form in A1, A2 and A3.

nucleation, the experiments were stopped and the crystals were extracted by dissolving the gel in a 1 M NaOH solution. All experiments were carried out at 25 °C.

The physicochemical conditions within the gel at nucleation time were estimated following the protocol described by Katsikopoulos et al.[15] In this approach, the concentration profiles of the reactants in the gel column can be calculated using a one-dimensional algorithm (eq 1), that is, assuming a linear diffusion model:[12,16]

$$C(d, t + \Delta t) = \text{mixf} \cdot C(d - \Delta d, t) + (1 - 2 \cdot \text{mixf}) \cdot C(d, t)$$
$$+ \text{mixf} \cdot C(d + \Delta d, t) \quad (1)$$

where C = reactant concentration, d = distance from the source reservoir, t = time, mixf = mixing factor, which depends on the porosity ($\varphi = 1.19$), the effective tortuosity of the gel ($\tau = 0.969$), and the diffusion coefficient of the reactant in water (Dw).[17,18] The calculations were carried out using the geochemical code PHREEQC, version.2.13,[19] which contains critical stability constants and diffusion coefficients of numerous solute species in water at 25 °C, its multicomponent-diffusion transport tool (MDT), and the PHREEQD.DAT database.

Morphological and Structural Characterization of CaCO₃ Crystals. Crystals with representative morphologies were hand-picked and studied using scanning electron microscopy (JEOL JSM6400, 40 kV) equipped with a LINK Ex1 energy dispersive spectrometer.

Raman spectra of the samples were collected using a confocal Raman microscope (WITec alpha 300 R) equipped with a SHG Nd:YAG laser (532 nm, max. power 22.5 mW) and a lens-based spectrometer. Elastically scattered photons were rejected by a long pass filter; that is, only the Stokes shifts were recorded. Using 600 and 1800 mm⁻¹ diffraction gratings, the spectral resolution was 3.5 and 1.2 cm⁻¹ per CCD-pixel, respectively. Spectra were recorded at selected positions with an integration time of 1, 5, and 10 s and 10-fold averaging at 5 mW. A 100× microscope objective (working distance 0.26 mm, NA 0.90) was used for the measurements. On the samples, two areas were selected under the microscope and 2−3 spots were analyzed from each area. The Raman bands of the CaCO₃ polymorphs have been discussed by Wehrmeister et al.[20] in detail. Thus, we follow their peak assignment.

Calcite crystals covering a wide range of morphologies and growth conditions were selected and further characterized by electron microprobe analysis and single crystal X-ray diffraction (SXRD). The calcite crystals were mounted in epoxy on glass slides, polished, carbon coated, and analyzed by a JEOL JXA 8900 microprobe. SXRD data were collected on a four-circle kappa diffractometer (Gemini, Oxford Diffraction, 50 kV, 40 mA) equipped with a CCD-detector (Atlas). For SXRD

Table 1. Concentrations of the Solutions Used in the Gel Experiments

mixture	[CaCl₂] (M)	[Na₂CrO₄] (M)	[Na₂CO₃] (M)
I	0.5		0.5
II	0.5	0.10	0.5
III	0.5	0.15	0.5
IV	0.5	0.20	0.5

measurements, the crystals were prepared by a pressurized air mortar to show a regular ellipsoidal form (200 μm in diameter). The data were collected by a Φ scan with a step of 1° in a 80 mm detector−crystal distance using MoK$_{\alpha 1}$ radiation up to a d-spacing range of 0.7−0.8 Å. Data collection and reduction including absorption correction according to Clark and Reid[21] were performed with the Oxford Diffraction data analysis software CrysAlisPro. Structure analyses and refinements were performed by direct methods and difference-Fourier synthesis, respectively, using SHELXL-97.[22]

■ RESULTS AND DISCUSSION

Influence of Cr(VI) on the CaCO₃ Polymorph Selection and Crystallization Sequence. In all experiments, the first crystals observable with 400× magnification occurred after ~240 h. The crystals first appeared ~7 cm from the calcium reservoir (branch A in Figure 1) within an area of ~0.5 cm in length (A1). With time, the length of the crystallization region increased to about 3.5 cm after two months.

Although chromate caused no change in the initial nucleation time and the location of the first precipitate, the number, size, and morphology of the crystals differed with respect to experiments with pure gel. The distribution of crystal morphologies in Cr(VI)-free experiments is depicted in Figure 2, while Figure 3 summarizes the results in chromate-bearing gels. According to the crystal morphology, three areas can be distinguished: A1, A2, A3. Crystallization occurs first in A1 (0.5 cm) and subsequently in A2 (1 cm) and A3 (2 cm).

For Cr(VI)-free experiments, rhombohedral single crystals occurred in all areas with slight morphological differences depending on their location (Figure 2). Crystals in A1 revealed dendritic branches (Figure 2b), while those in A2 and A3 evolved from hopper-shaped crystals (Figure 2c) to rhombohedra with flat faces (Figure 2a). Among the first nuclei in A1, a small number of spheres was also observed. These spheres dissolved shortly after their formation, while the rhombohedral crystals continued to grow. Irrespective of their morphology, all rhombohedral crystals revealed the same Raman spectrum (Figure 4a). We observed strong Raman bands at 156, 282, 711, and 1085 cm⁻¹ which clearly indicate calcite. All spectral lines of the CaCO₃ polymorphs and band-assignments are compiled in Table 2. Although no spheres could be recovered from the gel, the fact that they dissolved simultaneously with the growth of calcite crystals indicates a polymorph less stable than calcite, and according to their morphologies are most probably vaterite.

In chromate-bearing experiments, all areas contained rhombohedral single crystals. In A1 and A2, the rhombohedra were morphologically identical to those formed in Cr(VI)-free gels (c.f., compare Figure 3, panels c and g to Figure 2, panels b and c). However, the morphology of the rhombohedral crystals in A3 differed remarkably. These crystals were yellow and grew elongated along their 3-fold axis with curved prism surfaces (Figure 3a,b).
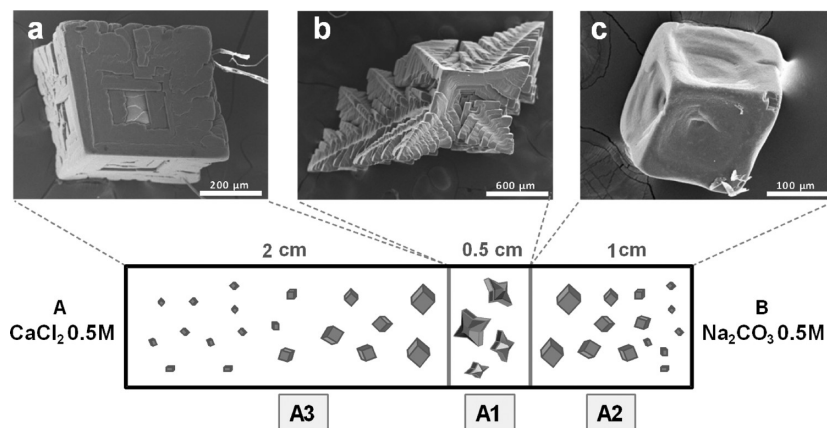
Figure 2. Typical sequences observed in Cr(VI)-free experiments 2 months after the first nucleation. At this time, the crystals were retrieved from the gel.

Raman spectra of the crystals formed in A1 and A2 showed the same features as the spectrum in Figure 4b confirming calcite. A Raman spectrum of an elongated rhombohedral crystal obtained from A3 is depicted in Figure 4c. The most prominent features of this spectrum also confirm calcite. However, additional peaks in the region between 800 and 1000 cm^{-1} cannot be assigned to calcite nor any other CaCO$_3$ polymorph. The origin of these bands will be discussed later.

In Cr(VI)-bearing gels, a significant amount of crystal aggregates formed in A1 and A2. These aggregates consisted of either radiating spherulitic (Figure 3e,f) or fibrous individuals (Figure 3d). Raman spectra from these aggregates are shown in Figure 5. All spectra collected from spherulitic individuals unambiguously show the typical vaterite triplet (symmetric stretching mode) at 1074, 1081, and 1094 cm^{-1} as well as the in-plane bending modes between 660 and 750 cm^{-1}. Moreover, the various translational and rotational lattice modes of vaterite can be easily identified between 100 and 300 cm^{-1} (Figure 5a). In contrast, fibrous individuals revealed Raman spectra of aragonite as shown in Figure 5b.

In A1, the type of polymorph, number, and mean size of crystals were determined 12 days after their initial nucleation. The data are presented in Table 3. The number of crystals can be considered as representative of the nucleation density. In Cr-(VI)-free gels, the first precipitate mainly consisted of calcite with less than 10% vaterite and no aragonite. In Cr(VI) containing gels, the suppression of calcite growth was clearly correlated with the chromate concentration. The nucleation density of vaterite and aragonite followed a trend opposite to that of calcite and strongly increased with the chromate concentration. At maximum chromate concentration, mainly vaterite and aragonite were found, whereas calcite represented merely ∼30%. The mean size of the crystals also decreased with increasing chromate concentration. This decrease was especially evident in the case of calcite. In gels with 0.2 M chromate, the size of calcite crystals was 50% of the size in control experiments.

The experiments show that chromate affected the nucleation density, the size, and the ratio of the precipitating polymorphs. In order to evaluate the extent of the chromate influence and to distinguish it from other parameters (such as supersaturation), information on the physicochemical conditions in the nucleation region at any time is required. Initially, the concentration of the reactants, Ca^{2+} and CO$_3^{2-}$, in the gel was zero and the distribution of chromate was homogeneous. Subsequently, counter-diffusion of reactants from the reservoirs and diffusion of chromate toward the columns induced concentration gradients within the column. If the diffusion of chemical species was progressing without crystallization, the gel column would become chemically homogeneous. The physicochemical evolution of the gel column can be modeled using PHREEQC, as explained in Section 2. Modeling of the system is limited to the time when the first precipitate is formed. Precipitates represent a sink for the reactants and affect diffusion.[12] The simulations are summarized in Figure 6.

Maximum concentrations of Ca^{2+} and CO$_3^{2-}$ existed close to the respective reservoirs and progressively decreased with increasing distance (Figure 6a). The CrO$_4^{2-}$ concentration varied in the central part of the gel column to some degree and strongly decreased near the reactant reservoirs (Figure 6b). The pH profile resulted from the concentration profile. The pH was ∼10 near the Na$_2$CO$_3$ reservoir, where the CO$_3^{2-}$ concentration was high, and decreased to 5.5 in the proximity of the CaCl$_2$ reservoir (Figure 6c). Figure 6d shows the supersaturation profiles for all experiments. Independent of the initial concentration of chromate in the gel column, the supersaturation profiles show a maximum at 6.5 cm distance from the CaCl$_2$ reservoir. The position of the first precipitate in the gel column was very close to this maximum and coincided with [Ca^{2+}]/[CO$_3^{2-}$] = 1 (Figure 6a). This is in good agreement with previous works.[12,13,23−27] The maximum supersaturation (Figure 6d) decreased from $\beta_{calcite}$ = 47 for the Cr(VI)-free experiment to $\beta_{calcite}$ = 27 for the 0.2 M chromate-bearing gel due to an increasing complexation of calcium by chromate. It is worth to note that in all the cases supersaturation was calculated with respect to pure calcite. The lack of thermodynamic data on Cr(VI)-bearing calcites made impossible to calculate the actual supersaturation of the solution with respect to calcites with different contents of Cr(VI). Nonetheless, it can be assumed that Cr(VI)-bearing calcites are more soluble than pure calcite. Consequently, supersaturation values with respect to Cr(VI)-bearing calcites should be lower than those presented in Figure 6d.

The differences in supersaturation cannot account for the differences in nucleation density, crystal sizes, and ratio of precipitating polymorphs. Considering the supersaturation profiles, the maximum nucleation density, the minimum crystal size, and the highest proportion of metastable polymorphs would be expected in the Cr(VI)-free experiment. The results showed the opposite (Table 3). It can be concluded that chromate inhibits the nucleation and growth of calcite and promotes the formation
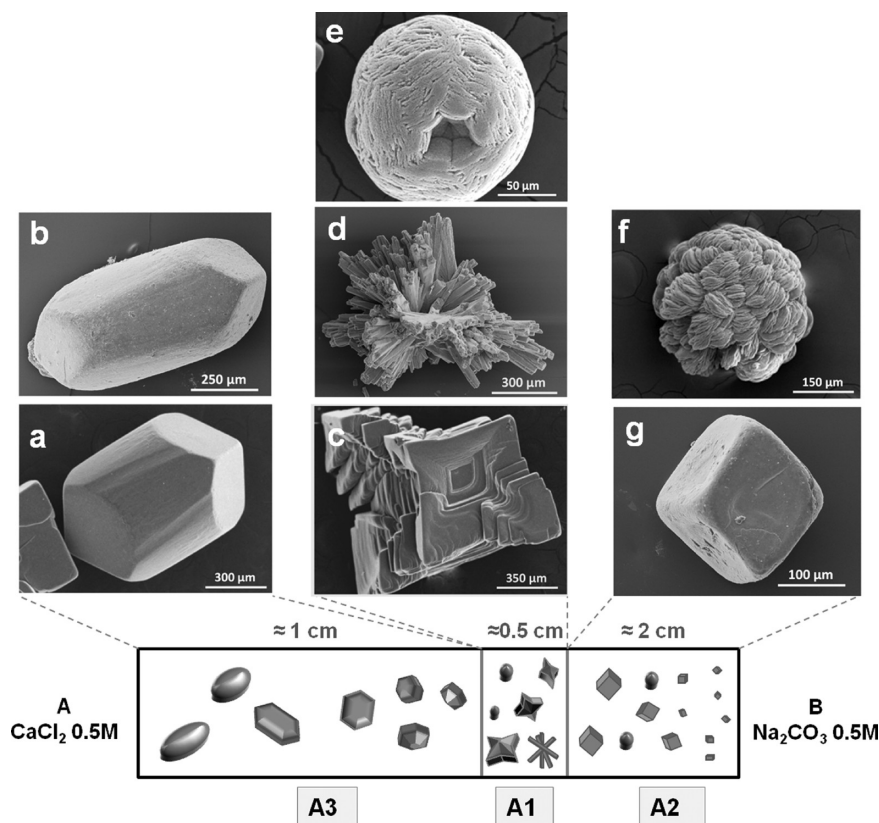
Figure 3. Typical sequence observed in the Cr-doped experiments 2 months after the first nucleation (when the crystals were retrieved from the gel).
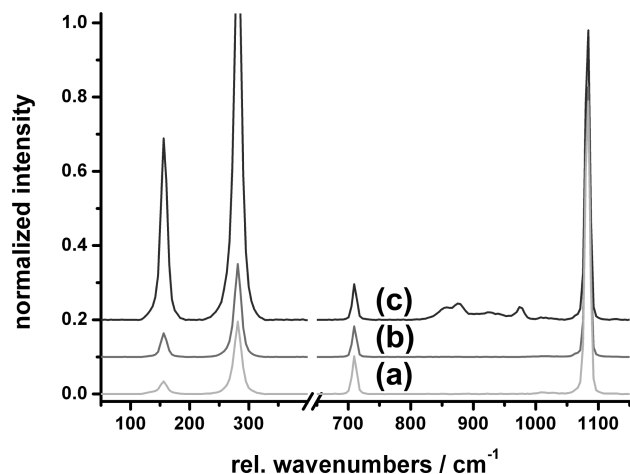

Figure 4. Raman spectra of crystals grown in the absence and in the presence of chromium. (a) Rhombohedral calcite crystals from A1, A2, and A3 in the control experiments. (b) Rhombohedral calcite crystals from A1 and A2 in the Cr-bearing experiments. (c) Elongated calcite crystals from A3 in the Cr-bearing experiments.

of metastable polymorphs. This is consistent with previous investigations. Hua et al.[8] reported a direct correlation between the amount of vaterite in $CaCO_3$ precipitates and the chromate concentration in an aqueous solution. The stabilization of metastable polymorphs, carbonate hydrates, or amorphous phases is not a unique property of chromate. Larsen[28] and Ito[29] related the formation of ikaite ($CaCO_3 \cdot 6H_2O$) to the presence of dissolved phosphate. It has also been suggested that

the phosphate ion can stabilize biogenic amorphous calcium carbonate (ACC) in the caparace of some animals.[30] Gal et al.[31] proposed that silicate ions play a similar role in the stabilization of biogenic ACC in cystholiths, the small calcified bodies produced by some plants. Kellermeier et al.[32] obtained ACC nanospheres by inorganic precipitation from silicate-rich solutions. Fernández-Díaz et al.[33] reported that high sulfate/carbonate ratios in aqueous solutions favors the formation of vaterite and inhibits its transformation into calcite. It is striking, however, that all these mentioned additives (including chromate) form tetrahedral anionic molecules.

Navrotsky[34] pointed out that calcite, aragonite, and vaterite are close enough in free energy that small changes in their surface properties and/or concentration of impurities can give rise to stability crossovers. The effect of tetrahedral anionic molecules on the crystallization of $CaCO_3$ might be related to the incorporation into their structures and/or to specific effects on the surface of the different polymorphs.

Isomorphic substitutions of anionic groups are not uncommon. For example, the $Ba(SO_4,CrO_4)$ (Barite-hashemite) solid solution is complete.[35] Substitutions of sulfate by selenate or arsenate were reported by Andara et al.[18] In these cases, the geometry of the anionic groups is identical, which eases substitution energetically. Carbonate is triangular planar. However, there is evidence that small amounts of tetrahedral molecules can incorporate into the structure of $CaCO_3$ phases. On the basis of the X-ray diffraction of natural calcites from biotic and abiotic origin, Busenberg and Plummer[36] concluded that sulfate can substitute carbonate. Similar conclusions were made for synthetic $CaCO_3$ precipitates.[33] Frisia et al.[37] corroborated the substitution of sulfate for carbonate groups in the calcite structure using synchrotron

Table 2. Overview of the Raman Vibrations Observed for the CaCO₃ Polymorphs[a]

| mode assignments	calcite	aragonite	vaterite
lattice modes	156, 282	152, 180, 192, 205, 247, 260, 271, 283	124, 153, 174, 213, 268, 277, 301, 332
in-plane bending	711	716	665, 683, 738, 744, 751
out-of-plane bending	/	854	/
symmetric stretching	1085	1085	1074, 1081, 1094

[a] Assignments follow Wehrmeister and co-workers.[20] Peak positions are given in cm^{-1}.

radiation-based techniques. Moreover, XANES and EXAFS analyses by Tang et al.[9] indicate that Cr in the calcite structure occurs as chromate, most probably substituting carbonate positions.

The Incorporation of Chromate into Calcite: Physicochemical Controlling Factors and Morphological Consequences. Some of the calcite crystals of the Cr-bearing experiments had shapes different from {104} rhombohedra, a yellow shading, and additional bands in their Raman spectra. These features point toward an incorporation of chromate. In order to elucidate this possibility, different types of calcite crystals have been investigated further.

As explained above, all calcite crystals formed in Cr(VI)-free experiments were rhombohedra bounded by the most stable {104} faces.[38] Crystals in A1 showed signs of dendritic growth. This likely was a consequence of the high supersaturation in this region at least during nucleation and the initial stages of growth. The faces of rhombohedral crystals in A1 and A2 evolved from hopper to flat faces. Because crystals in A1 represented a sink for Ca^{2+} and CO_3^{2-}, the nucleation in A2 and A3 occurred at lower supersaturation levels. As growth progressed, supersaturation decreased due to the consumption of reactants. This lead to a change in the growth mechanism from a two-dimensional nucleation to a spiral growth. This change can account for the evolution of calcite crystals in A2 and A3. Similar explanations for the spatial and temporal evolution of the habit of calcite crystals grown in silica gel were provided by a number of authors.[13,26,39]

The morphology of the calcite crystals growing in A1 and A2 of the chromate-bearing gels can also be explained based on supersaturation evolution. However, supersaturation cannot account for the characteristics of calcite crystals in A3. The morphology of these crystals deviates from the normal {104} rhombohedron. As shown in Figure 3a,b, these crystals are elongated along the c axis, with curved surfaces in the prism region and terminated by {104} faces. Their degree of elongation varies within a wide range, with length/width (L/W) ratios between 1.1 and 2.2, independent from the initial chromate concentration in the gel although their mean length decreases with increasing initial chromate concentration (0.85 mm for 0.1 M and 0.52 mm for 0.2 M chromate concentration). Moreover, within the same gel column, the (L/W) ratio increases toward the CaCl₂ reservoir (see calcite habit A3a and A3b in Figure 3). These crystals show a yellow color whose intensity directly correlates
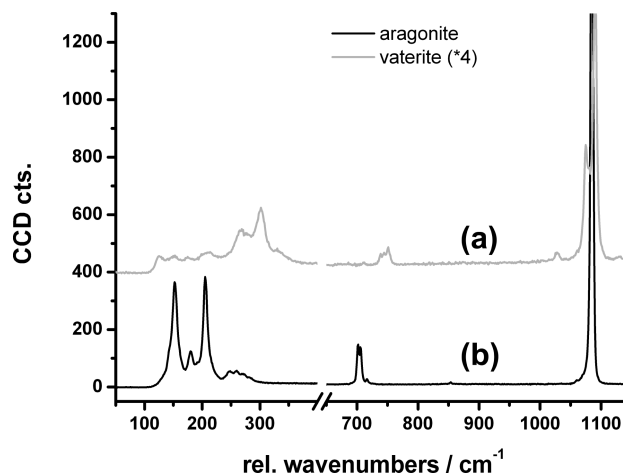
Figure 5. (a) The Raman spectrum taken from spherulitic aggregates is showing characteristic peaks of vaterite. (b) In contrast, the spectrum of fibrous aggregates matches with that of aragonite. In general, Raman scattering intensities in aragonite were around four times larger than in vaterite. The vaterite spectrum was maximized four times (*4) for a better comparison.

with their L/W ratio. The physicochemical parameters depicted in Figure 6 show that crystals in A2 and A3 form under similar supersaturations. The main differences depend on the ratio between the relevant chemical species and pH. Because pH controls the distribution of dissolved carbon between CO_3^{2-}, HCO_3^-, and H_2CO_3, the CrO_4^{2-}/CO_3^{2-} ratio was low in the region of the gel column where the pH was high, that is, close to the Na₂CO₃ reservoir (Figure 1), and vice versa. Figure 7 shows the distribution of CrO_4^{2-}/CO_3^{2-} ratio values along the gel column for the 0.2 M bearing chromate experiments at nucleation time. The inset shows the value of this ratio in the crystallization region (5–8.5 cm). As can be seen, yellow elongated calcite crystals only appeared in the region where CrO_4^{2-}/CO_3^{2-} > 70. Moreover, within A3, the L/W ratio varied between 1.1 and 1.25 where 360 > CrO_4^{2-}/CO_3^{2-} > 70 (A3a) and between 2 and 2.2 where CrO_4^{2-}/CO_3^{2-} > 360 (A3b). Therefore, it can be concluded that the CrO_4^{2-}/CO_3^{2-} ratio was the factor that most strongly controlled the variation in habit when calcite formed in the presence of chromate.

The morphology of calcite crystals in A3 of chromate-bearing gels was similar to that observed with SO_4^{2-} or HPO_4^{2-} as additives.[33,40,41] Parker et al.[42] and Titiloye et al.[43] used molecular dynamics to predict the effect of HPO_4^{2-} on calcite morphology. According to these authors, hydrophosphate selectively segregates on the {100} faces due to a combination of strong binding and minimal steric hindrance. As a result, the predicted morphology is a first-order prism capped with rhombohedral end faces. A similar mechanism can explain the effect of the chromate on calcite morphology.

Raman spectra of elongated yellow calcites from gels with different initial chromate concentrations are shown in Figure 8. In addition to those bands characteristic for calcite (Table 2), all spectra show weak bands between 850 and 925 cm^{-1}. The inset in Figure 8 shows a close up of this region with the main vibrational modes for chromatite (CaCrO₄) for comparison. The chromatite spectrum was obtained from a natural sample.

Among the CaCO₃ polymorphs, only aragonite reveals a peak at approximately 853 cm^{-1}. For calcite, such a peak is not

Table 3. Crystal Density (cd) and Mean Size of Calcite (C), Vaterite (V), and Aragonite (A) Individuals Formed in A1 Measured 12 Days after the Formation of the First Nuclei
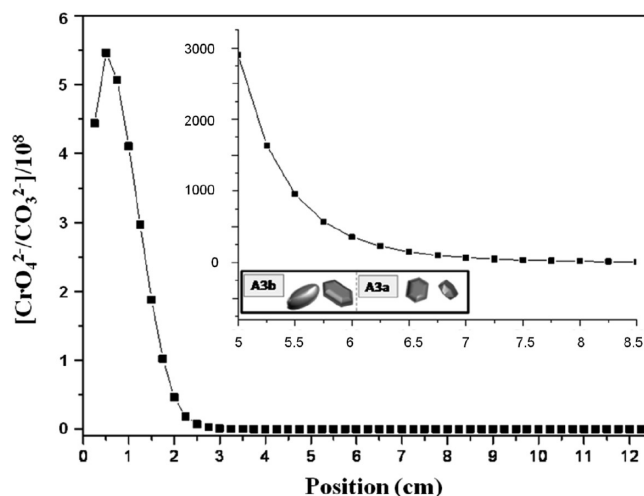
			AREA 1 (12 days after nucleation)			
	$C - cd^a$	$C - size$ (mm)	$V - cd^a$	$V - size$ (mm)	$A - cd^a$	$A - size$ (mm)
pure system	17	1.25 × 0.75	2	0.75 Ø		
0.10 M Cr	15	1 × 0.5	4	0.25 Ø	5	0.62 Ø
0.15 M Cr	12	0.62 × 0.5	6	0.25 Ø	8	0.5 × 0.2
0.20 M Cr	10	0.5 × 0.37	10	0.2 Ø	12	0.3 × 0.12

^{a} Number of crystals observable with 400× magnification.
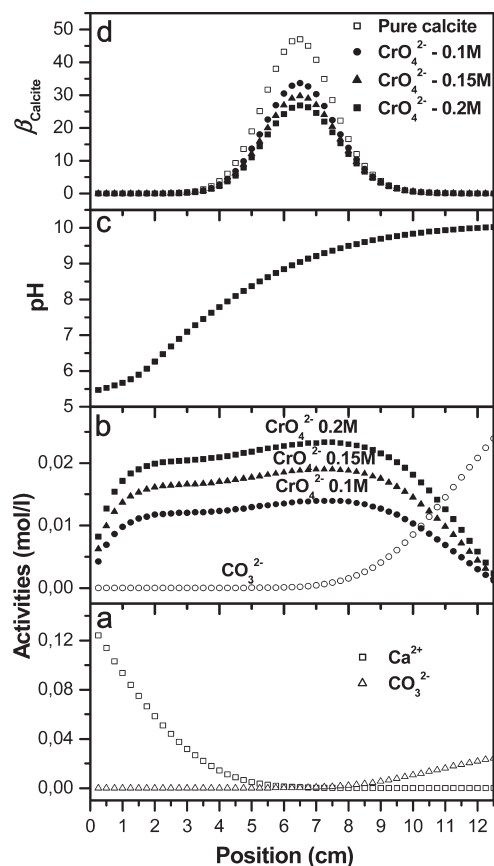
Figure 6. Activity profiles at the moment of nucleation of the first crystal modeled using PHREEQC. (a) Concentration profiles of Ca^{2+} and CO_3^{2-} ions, (b) concentration profiles of CO_3^{2-} and CrO_4^{2-} ions, (c) pH profile, and (d) supersaturation with respect to calcite along the diffusion column.

Figure 7. Distribution of the CrO_4^{2-}/CO_3^{2-} ratio along the gel column for the 0.2 M bearing chromate experiments at nucleation time. The inset shows the value of this ratio in the crystallization region.
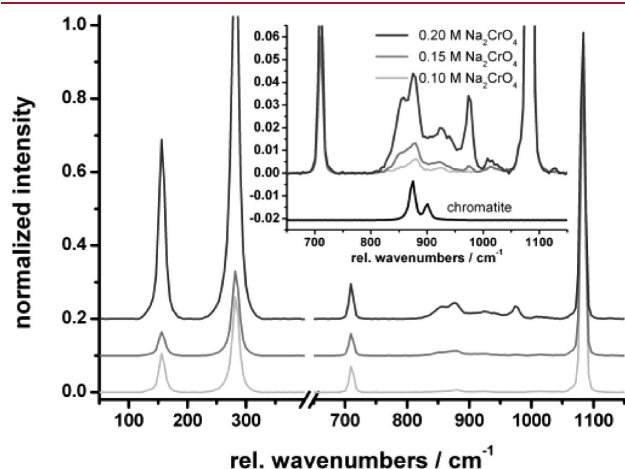
expected. However, this vibrational mode also corresponds to the most prominent band of chromatite at 875 cm^{-1} (CrO_4 symmetric stretching). Some additional weak bands are also present. Wilkins[44] reported that the Raman spectrum of crocoite gives three bands in the CrO stretching region at 825, 838, and 853 cm^{-1}. Frost[45] showed the Raman spectra of the CrO stretching region of some chromate-bearing minerals with a varying position from 825 to 972 cm^{-1} depending on the mineral. In our experiments, we observed three main bands at 858, 875, and 974 cm^{-1}. The first two bands are in agreement with the peak positions reported by Frost[45] and, subsequently, the new bands can be a consequence of the incorporation of Cr(VI) into the calcite structure as chromate groups. Furthermore, Wang

et al[46] conducted a Raman spectroscopic study to distinguish the chromate species on Cr-MCM-41 synthesized by direct hydrothermal synthesis. There, the color of the samples was pale green and it changed to pale yellow after the calcinations suggesting the change of the oxidation state of the Cr species from Cr^{3+} to Cr^{6+}. The band at 980 cm^{-1} was assigned to the Cr–O vibration stretching of the dehydrogenated monochromate species (CrO_4^{-2}). Thus, the third more intense band that we observed in our data can also be correlated with the presence of Cr(VI) incorporated into the calcite structure. This is supported by the fact that the intensity of the new bands correlates with the initial content of chromate in the growth medium.

Pale yellow calcite crystals were chosen for SXRD studies, and these were compared to pure calcite. Reconstructed reciprocal planes of all data sets display no forbidden reflections which do not belong to $R\bar{3}c$, except for weak reflections due to $\lambda/2$ at small Bragg angles (Figure 9).

In order to check the hypothesis that chromate was incorporated into the yellow calcite crystals, their structures were determined, refined, and compared to the refined structure model of pure calcite: C sites for each structures could be easily found by the difference Fourier analysis, after the determination of Ca and O positions by direct methods. In order to prove the substitution of $(CrO_4)^{4-}$ for $(CO_3)^{2-}$, in the last cycle of refinement, the occupancy parameter of C was calculated using fixed anisotropic atomic displacement parameters (ADPs in [Å^2]) with values that had been obtained by analyzing our SXRD

data of pure calcite: $U_{11} = 0.01074$ [Å^2]; $U_{22} = 0.01074$ [Å^2]; $U_{33} = 0.01037$ [Å^2]; $U_{12} = 0.00537$ [Å^2]. The resulting occupancy parameters showed more than 100% occupancies, indicating partial substitution of Cr(VI) for C. From the resulting occupancies, the weight percentages of Cr(VI) between 2667 ppm and 6667 ppm could be estimated as given in Table 4. These values cannot be the correct portion of $(CrO_4)^{4-}$ substituting for $(CO_3)^{2-}$ in our yellow calcite crystals due to the fixed ADPs in the refinements. However, the higher occupancy parameters refined for yellow calcite structures compared to that of the pure calcite indirectly point to the incorporation of $(CrO_4)^{4-}$ in the calcite lattice.
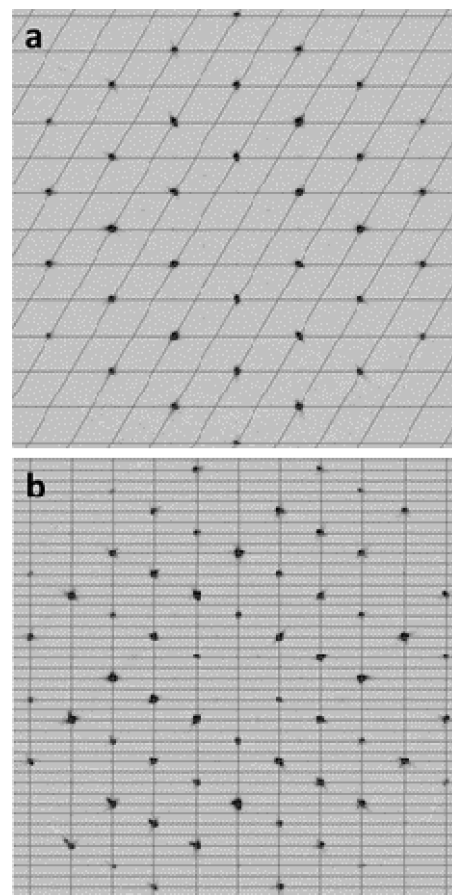
Electron microprobe analyses of the elongated yellow samples (area A3) obtained from the chromium bearing experiments yielded similar results as those derived from the SXRD study. The chromate concentration obtained for those samples varied depending on the Cr concentration in the growth medium, and it was (1900 ± 300) ppm, (3800 ± 500) ppm, and (5900 ± 400) ppm for calcite crystals grown in the presence of 0.1 M, 0.15 M, and 0.2 M of chromium. Both SXRD and microprobe results indicate a direct correlation between the Cr(VI) content of the yellow calcites and the initial chromate concentration in the gel. According to our results, chromate was incorporated into the calcite structure isomorphically by substituting carbonate. This substitution was restricted by the different geometry of the chromate molecule and the carbonate group, which likely caused local strain.

$[CrO_4^{2-}]/[CO_3^{2-}]$ ratios plotted in Figure 7 exclusively represent the values at nucleation time. As crystallization progresses, this ratio changes due to the coupling between mass transfer from and toward the reservoirs and reagent consumption by the growing crystals. Although the lack of information on the extension of this coupling makes it impossible to obtain reliable $[CrO_4^{2-}]/[CO_3^{2-}]$ ratios in the region of the gel column and at the time of calcite crystal formation, we can use the $[CrO_4^{2-}]/[CO_3^{2-}]$ ratios at nucleation time as reference values. By comparing $[CrO_4^{2-}]/[CO_3^{2-}]$ ratios in the calcite crystals

Figure 8. Comparison of the Raman spectra corresponding to calcite crystals with deep yellow color from the experiment with 0.1, 0.15, and 0.2 M Na$_2$CrO$_4$ in the gel. The inset shows a close up view of the chromate induced peaks.

Figure 9. (a) Reconstructed reciprocal $hk0$ and (b) $h0l$ planes from SXRD data.

Table 4. Refined Structure Parameters of the Pure and Yellow Crystals Obtained from the Area A3 in the Cr-Doped Experiments

refined parameter	CaCO$_3$ pure	CaCO$_3$ − Cr 0.1 M	CaCO$_3$ − Cr 0.15 M	CaCO$_3$ − Cr 0.20 M
a [Å]	4.9885(1)	4.9866(2)	4.9869(2)	4.9864(2)
c [Å]	17.0729(3)	17.0613(6)	17.0554(8)	17.0592(6)
V [Å^3]	367.9	367.4	367.3	367.3
# unique reflections	153	110	108	153
R_{int} [%]	3.72	1.16	1.84	2.25
wR_2 [%]^a	4.36	4.03	4.01	3.82
goodness-of-fit	1.34	1.33	1.31	1.32
occupancy for the C position [0.1667 ≅ 100%]	0.1667	0.168(2)	0.169(2)	0.170(1)
amount Cr at the site for C [ppm]	**0**	**2667(32)**	**4667(55)**	**6667(39)**

^{a} Weight $= 1/[\sigma^2(F_o^2) + (a*P)^2 + b*P]$ where $P = (\text{Max}(F_o^2, 0) + 2*F_c^2)/3$; with the observed and calculated structure factor F_o and F_c, respectively, and the refined a and b values during the analysis.

(in ppm) and in the fluid (in mM), apparent Cr(VI) partitioning coefficients (K_d) are obtained, according to the following equation:[36]

$$K_d = [CrO_4^{2-}/CO_3^{2-}]_{solid}/[CrO_4^{2-}/CO_3^{2-}]_{solution} \quad (2)$$

The average calculated apparent partition coefficient is ~10 in all the experiments. However, apparent partition coefficients strongly vary in a given experiment, with values ranging from ~2, in the region where the calcite and the aqueous solution $[CrO_4^{2-}]/[CO_3^{2-}]$ ratios are lower (region A3a in Figure 7) to ~20, in the region where the calcite and the aqueous solution $[CrO_4^{2-}]/[CO_3^{2-}]$ ratios are higher (region A3b in Figure 7). It is important to note that the partitioning coefficients calculated in this way necessarily are inaccurate because their value can be strongly affected by factors such as supersaturation, growth rate, and Cr(VI) depletion during growth, which cannot be controlled. Moreover, the distribution of Cr(VI) in the calcite crystals is not homogeneous. However, it is striking that the average apparent partition coefficient reported in this work (~10) coincides with that obtained by Tang et al[9] in batch coprecipitation experiments when $[Cr]_{solution} > 10$ mM. Therefore, it can be concluded that our result reasonably estimates Cr(VI) partitioning in strongly contaminated media when mass transfer is restricted.

CONCLUSIONS

The presence of a toxic pollutant such as Cr(VI) in the crystallization medium has an important influence on both the nucleation and the growth of $CaCO_3$. Regarding the nucleation, it can be concluded that Cr(VI) (i) promotes the formation of vaterite and aragonite, which form in a higher proportion in Cr(VI)-bearing experiments compared to Cr(VI)-free experiments and (ii) reduces the nucleation density of calcite proportionally to the Cr concentration in the medium. Regarding the influence of Cr(VI) on the growth of $CaCO_3$ polymorphs, we observed that with an increasing concentration of Cr(VI) in the medium (i) the mean size of single crystals and aggregates decreases, (ii) the habit of calcite crystals changes from {104} to forms elongated along the c-axis, and (iii) the amount of incorporated Cr increases. This incorporation is evidenced by the appearance of additional vibrational bands in the Raman spectra. The location of these bands is consistent with the substitution of carbonate groups by chromate groups.

The coprecipitation of chromate with calcium carbonate is a likely process when calcite forms in media strongly contaminated by chromate, especially when mass transfer is restricted. This incorporation can significantly affect the biological availability of this pollutant in natural environments. Moreover, the apparent partitioning coefficients of Cr(VI) into calcite determined in this work suggest that $CaCO_3$ precipitation processes have the potential to significantly influence the fate of this pollutant in natural environments.

AUTHOR INFORMATION

Corresponding Author
*Tel: +34-91-394-4884. Email: nsanchez@geo.ucm.es.

ACKNOWLEDGMENT

REFERENCES

(1) Katz, S. A.; Salem, H. In *The Biological and Environmental Chemistry of Chromium*; VCH: New York, 1994.

(2) Traina, S. J.; Laperche, V. *Proc. Natl. Acad. Sci. U. S. A.* **1999**, *96*, 3365–3371.

(3) Prieto, M.; Cubillas, P.; Fernandez-Gonzalez, A. *Geochim. Cosmochim. Acta* **2003**, *67*, 3859–3869.

(4) Pérez-Garrido, C.; Fernández-Díaz, L.; Pina, C. M.; Prieto, M. *Surf. Sci.* **2007**, *601*, 5499–5509.

(5) Godelitsas, A.; Astilleros, J.M .; Hallam, K.; Harissopoulos, S.; Putnis, A. *Environ. Sci. Technol.* **2003**, *37*, 3351–336.

(6) Garelick, H.; Dybowska, A.; Valsami-Jones, E.; Priest, N. D. *J. Soils Sediments* **2005**, *5*, 182–190.

(7) Sneedon, I. R.; Orueetxebarria, M.; Hodson, M. E.; Schofield, P. F.; Valsami-Jones, E. *Environ. Pollut.* **2006**, *144*, 816–825.

(8) Hua, B.; Deng, B. L.; Thorton, E. C.; Yang, J.; Amonette, J. E. *Water, Air, Soil Pollut.* **2007**, *179*, 381–390.

(9) Tang, Y. Z.; Elzinga, E. J.; Lee, Y. J.; Reeder, R. J. *Geochim. Cosmochim. Acta* **2007**, *71*, 1480–1493.

(10) Henisch, H. K. In *Crystals in Gels and Liesegang Rings*; Cambridge University Press: New York, 1988.

(11) Putnis, A.; Prieto, M.; Fernández-Díaz, L. *Geol. Mag.* **1995**, *132* (1), 1–13.

(12) Henisch, H. K.; García-Ruiz, J. M. *J. Cryst. Growth* **1986**, *76*, 203–211.

(13) Prieto, M.; Fernández-Díaz, L.; López-Andrés, S. *J. Cryst. Growth* **1989**, *98*, 447–460.

(14) Sánchez-Pastor, N.; Pina, C. M.; Fernández-Díaz, L. *Chem. Geol.* **2006**, *225*, 266–277.

(15) Katsikopoulos, D.; Fernández-González, A.; Prieto, M. *Min. Mag.* **2009**, *73*, 269–284.

(16) Appelo, C. A. J.; Postma, D. In *Geochemistry, Groundwater and Pollution*, 2nd ed.; A. A. Balkema Publishers: Leiden, The Netherlands, 2005.

(17) Oelkers, E. In *Physical and Chemical Properties of Rocks and Fluids for Chemical Mass Transfer Calculations*; Lichtner, P. C., Steefel, C. I. Oelkers, E. H., Eds.; Reviews in Mineralogy, Mineralogical Society of America: Chantilly, Virginia, USA, 1996; Vol. 34, p 131.

(18) Andara, A.; Heasman, D. M.; Fernández-González, A.; Prieto, M. *Cryst. Growth Des.* **2005**, *5*, 1377–1378.

(19) Parkhurst, D. L.; Appelo, C .A . J. In *User's guide to PHREEQC (Version 2): A Computer Program for Speciation, Batch-Reaction, One-Dimensional Transport and Inverse Geochemical Calculations*; U.S. Geological Survey Water Resources Investigations Report; U.S. Geological Survey: Washington, DC, 2003.

(20) Wehrmeister, U.; Soldati, A. L.; Jacob, D. E.; Häger, T.; Hofmeister, W. J. *Raman Spectrosc.* **2010**, *41*, 193–201.

(21) Clark, R. C.; Reid, J. S. *Acta Crystallogr.* **1995**, *A51*, 887–897.

(22) Sheldrick, G. M. In *SHELXL-93, Program for the Refinement of Crystal Structures*; University of Göttingen: Göttingen, Germany, 1993.

(23) Prieto, M.; Putnis, A.; Fernández-Díaz, L. *Geol. Mag.* **1990**, *127*, 485–617.

(24) Prieto, M.; Fernández-Díaz, L.; López-Andrés, S. *J. Cryst. Growth* **1991**, *108*, 770–778.

(25) Prieto, M.; Putnis, A.; Fernández-Díaz, L.; López-Andrés, S. *J. Cryst. Growth* **1994**, *142*, 225–235.

(26) Putnis, A.; Prieto, M.; Fernández-Díaz, L. *Geol. Mag.* **1995**, *132*, 1–13.

(27) Fernández-Díaz, L.; Putnis, A.; Prieto, M.; Putnis, C. V. *J. Sediment. Res.* **1996**, *66*, 482–491.

(28) Larsen, D. *J. Sediment. Res.* **1994**, *64*, 593–603.

(29) Ito, T. *J. Min. Pet. Econ. Geol.* **1996**, *91*, 209–219.

(30) Al-Sawalmih, A.; Li1, C.; Siegel, S.; Fratzl, P.; Paris, O. *Adv. Mater.* **2009**, *21*, 4011–4015.

(31) Gal, A.; Weiner, S.; Addadi, L. *J. Am. Chem. Soc.* **2010**, *132*, 13208–13211.

(32) Kellermeier, M.; Melero-García, E.; Glaab, F.; Klein, R.; Drechsler, M.; Rachel, R.; García-Ruiz, J. M.; Kunz, W. *J. Am. Chem. Soc.* **2010**, *132* (50), 17859–66.

(33) Fernández-Díaz, L.; Fernández-González, A.; Prieto, M. *Geochim. Cosmochim. Acta* **2010**, *74*, 6064–6076.

(34) Navrotsky, A. *Proc. Natl. Acad. Sci. U. S. A.* **2010**, *101* (33), 12096–12101.

(35) Prieto, M.; Fernández-González, A.; Putnis, A.; Fernández-Díaz, L. *Geochim. Cosmochim, Acta.* **1997**, *61* (16), 3383–3397.

(36) Busenberg, E.; Plummer, N. *Geochim. Cosmochim. Acta* **1985**, *49*, 713–725.

(37) Frisia, S.; Borsato, A.; Fairchild, I. J.; Susini, J. *Earth Planet. Sci. Lett.* **2005**, *235*, 729–740.

(38) Heijnen, W. M. M. *N. Jb. Miner. Mh.* **1985**, *8*, 357–362.

(39) Fernández-González, A.; Prieto, M.; Putnis, A.; López-Andrés, S. *Mineral. Mag.* **1999**, *63*, 331–343.

(40) Fernández-Díaz, L.; Pina, C. M.; Astilleros, J. M.; Sánchez-Pastor, N. *Am. Mineral.* **2009**, *94*, 1223–1234.

(41) Suzuki, T.; Inomata, S.; Sawada, K. *J. Chem. Soc. Faraday Trans.* **1986**, *82*, 1733–1743.

(42) Parker, S. C.; Titiloye, J. O.; Watson, G. W. *Phil. Trans. R. Soc. Lond. A* **1993**, *344*, 37–44.

(43) Titiloye, J. O.; Parker, S. C.; Mann, S. *J. Cryst. Growth* **1993**, *131*, 533–545.

(44) Wilkins, R. W. T. *Min. Mag.* **1971**, *38*, 249–1971.

(45) Frost, R. L.; Weier, M. *Neues Jahrb. Mineral., Monatsh* **2004**, *12*, 575–594.

(46) Wang, Z.; Wilson, G. F.; Griffith, L. C. *J. Biol. Chem.* **2002**, *277* (27), 24022–24029.